Two-photon luminescence of gold nanorods: applications to single-particle tracking and spectroscopy

Carozza, S.

Chapter 1

Introduction

Imaging single molecules in live cells reveals details of cellular processes that cannot be seen using traditional averaging techniques. A proper choice of the microscope and the labels is essential to get the best results from a single-molecule imaging experiment. In this thesis we used gold nanorods for applications in single-particle imaging, tracking and spectroscopy, using a two-photon multifocal scanning microscope. A two-photon microscope is advantageous due to the possibility to image deep in the sample and the limited photodamage induced in cells by using low-energy photons. As labels, gold nanorods have great potential due to their high brightness and photostability and can be excited in two-photon.

This chapter introduces single-molecule imaging and summarizes the most common labels and microscopes used for these experiments. Then, we present the principles of two-photon excitation and discuss more in detail its advantages over one-photon excitation. We present the structures of a typical two-photon microscope and of the particular two-photon multifocal scanning microscope that we used for our experiments. Finally, we describe noble metal nanoparticles and explain the optical properties that make them such a powerful tool for single-molecule imaging.

1.1 Single-molecule imaging

This section introduces SM imaging experiments and gives a brief overview of the possible labels and imaging techniques to use for these experiments.

Cells are the basic structural and functional unit of all living organisms, and all processes occurring inside and between cells, such as gene replication, growth, diseases and immune defense, are regulated by particular molecules in the cells, mainly proteins and nucleic acids. For a deep understanding of cellular processes, it is necessary to study them at the single molecule level. Following each individual molecule reveals the distribution of all possible behaviors instead of only a population average. This way, intermediate states, rare events and non-synchronized processes within the sample can also be detected. The advantages of SM techniques are particularly valuable in live cells, where large spatial and temporal variations occur.

The first optical detection of a single molecule was achieved by Moerner in 1989, measuring the absorption of pentacene [1]. In 1990, Orrit and Bernard detected the fluorescence signal emitted by single molecules for the first time [2].These experiments were performed at cryogenic temperatures, where the absorption cross-section of fluorophores increases by several orders of magnitude and the suppression of thermal vibrations makes molecules more stable relative to room temperature. Thanks to new high-sensitivity detectors, such as avalanche photodiodes and charge-coupled devices, the weak signals from single fluorophores could later be detected also at room temperature. In 1995 Funatzu [3] visualized the movement of single proteins *in vitro*. Since then, SM imaging techniques became more and more common, and were for example applied to the study of protein dynamics [4], diffusion in phospholipid membranes [5] and cell signaling [6]. From 2000 SM experiments started to be applied *in vivo*: single receptor proteins were tracked on cells surface [7] and inside living cells [8].

1.1.1 Probes and labeling

As most biomolecules do not fluoresce by themselves, light-emitting probes are used to label and follow the molecules of interest. In live cells

many structures naturally absorb and emit light, giving a high background. An accurate choice of labels and imaging techniques is therefore essential to distinguish the weak signal of single molecules from the background. There are three main classes of probes: fluorescent proteins, organic dyes and fluorescent nanoparticles.

Fluorescent proteins (FPs) [7, 9, 10] present good biocompatibility and labelling specificity, as they can be encoded in the gene corresponding to the target protein. However, they have small optical cross-section and suffer from photobleaching. The performance of fluorescent proteins in SM imaging is thus limited: the weak signal limits the localization precision and photobleaching limits the measurement time.

Organic dyes are smaller than proteins, brighter, and cover a wider spectral range [11]. They are more stable than FPs but also suffer from photobleaching.

Nanoparticles, such as quantum dots (QDs) [12], are the most bright and stable among probes. However, they are larger than FPs and organic dyes and can thus influence the movement of the molecule of interest. In addition, QDs are prone to photoblinking. Noble metal nanoparticles, such as gold and silver nanospheres and nanorods, are brighter than QDs and do not bleach nor blink. Therefore they are a good choice to image molecules in cells with high spatial resolution and for long time.

Labeling proteins with organic dyes and nanoparticles is more challenging than genetic encoding of FPs. First, dyes and nanoparticles must be introduced into the cells using methods such as microinjection, electroporation or incubation. Then they must bind to the target protein. Mediating tags, usually proteins and small peptides, can be encoded in the gene of the target protein, and bind to the label upon expression [13].

Single-molecule techniques using nanoparticles are commonly referred to as single-particle (SP) techniques. In the work presented in this thesis we used gold nanorods for single-particle imaging, tracking and spectroscopy applications. A detailed discussion on gold nanoparticles, gold nanorods and their optical properties is presented in Section 1.3.

1.1.2 Single-molecule microscopy

SM imaging experiments typically use inverted microscopes, in wide-field or confocal configuration. In a wide-field microscope [3, 14] a wide area

of the sample is illuminated. To this aim, an expanded beam is focused on the back focal plane of the objective, resulting in a collimated beam that uniformly illuminates the sample. The fluorescence signal emitted by the sample as well as the reflected excitation light are collected by the same objective and separated by a dichroic mirror before imaging with a CCD (charge-coupled device) or a CMOS (complementary metal-oxide semiconductor) camera. This way, however, a large volume is excited and the fluorescence coming from out-of-focus z planes adds to the in-focus signal, compromising the signal to background.

To reduce the excitation volume, wide-field illumination can be obtained by total internal reflection fluorescence (TIRF) [15]: the excitation beam is focused on the back focal plane of the objective, but off-centered. This results in a slanted excitation beam and when the inclination angle exceeds a critical angle it generates an evanescence wave that decays exponentially from the glass interface. Only a thin slice of the sample (about 250 nm) is excited, avoiding the out-of-focus signal. This technique can be used to image thin samples, but it is not suitable, for example, to image several microns inside cells.

Confocal microscopes limit out-of-focus fluorescence by using a highly focused spot to excite a point inside the sample. The light is collected by the same objective, filtered with a dichroic, and a pinhole is used to reject the out-of-focus signal. Confocal microscopy provides a better signal-to-noise ratio compared to wide-field microscopy, due to the limited excitation volume and the use of avalanche photo-detectors that exhibit less dark counts and a higher quantum yield. It can excite deeper inside the sample, making 3D imaging possible. Nevertheless, the image is acquired only one spot at the time and scanning the excitation beam through the sample significantly slows down the imaging process.

In summary, to investigate cellular processes over extended periods of time and with high accuracy we ideally need small, stable and bright labels and fast 3D microscopes. A compromise must be made between the small but weak and unstable FPs and organic dyes, and bright and stable, large nanoparticles. Likewise, an optimum must be found in terms of 3D penetration, out-of-focus fluorescence and acquisition speed to obtain the highest signal and resolution.

1.2 Two-photon microscopy

1.2.1 Principles of two-photon excitation

For our experiments, we decided to use gold nanorods and a special multifocal two-photon scanning microscope.

The microscopy techniques we presented previously are based on the excitation of fluorescent probes by the absorption of one photon that brings an electron to a higher energy state. After rapid thermal relaxation, the electron falls back to the ground state while emitting a photon with an energy equal to the difference between the two levels minus some relaxation energy (Fig. 1.1a). As the excitation is realized by absorption of one photon at the time, we refer to these techniques as one-photon excitation (OPE) techniques.

Simultaneous absorption of two photons can also induce fluorescence excitation. The electron excitation occurs by absorption of two photons whose combined energy equals the energy gap between the ground state and the excited state. This process is called two-photon excitation (TPE). The absorption of the two individual photons must occur within about 0.5 fs [16]. After excitation, the electron follows the same decay pathway as in OPE (Fig. 1.1b).

Using TPE has several advantages over OPE [17]. The excitation wavelength shifts from the visible region in the spectrum to the near infared (nIR), because both photons carry half the energy. Larger wavelength photons are preferable for *in vivo* imaging, because they are absorbed less by cells and tissues and thus induce less photodamage. The lower absorption of photons by the sample allows for two to up to ten time deeper penetration in the sample than OPE [18, 19]. Moreover, there is a larger spectral gap between the excitation and emission wavelengths than in OPE and the two can better be separated, resulting in a weaker background signal. Another advantage of TPE is that the fluorescence signal scales with the square of the excitation intensity. As a consequence, the absorption is better confined (Fig. 1.2a) and out-of-focus absorption and fluorescence are strongly reduced (Fig. 1.2b). This yields an improvement in signal-to-noise ratio and sectioning in the z direction.

However, the TP absorption cross-section of fluorophores is far smaller

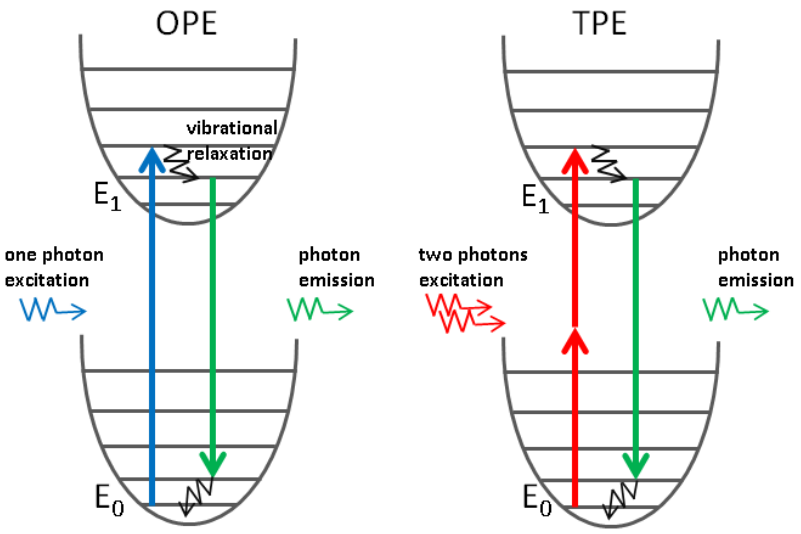

Figure 1.1
Jablonsky diagram for a) one-photon and b) two-photon fluorescence, showing the electronic states of a molecule and the transitions triggered by the excitation. The electronic levels of the molecules (E_0= ground state, E_1= first excited state) are represented as wells containing vibrational sub-levels.

than their OP cross-section and a high density of photons in short time is required for the excitation. As a result, photobleaching is more severe than in OPE [22]. As discussed in section 1.3, this is not limiting when metal nanoparticles are used.

1.2.2 Two-photon microscopes

To generate the high density of photons in short time that is required for TPE, titanium-sapphire (Ti-Sa) lasers are typically used. Ti-Sa lasers generate 100 fs pulse trains with wavelengths from 700 to 1000 nm at a rate of about 100 MHz [23].

Besides the nIR excitation source, a TP microscope is similar to a typical confocal microscope [17, 21], though the non-linear response alleviates the need for using a pinhole. Fig. 1.3 shows the typical scheme of a TP microscope. The beam diameter is increased using a telescope, and the light intensity can be controlled using a $\lambda\backslash 2$ plate and a polar-

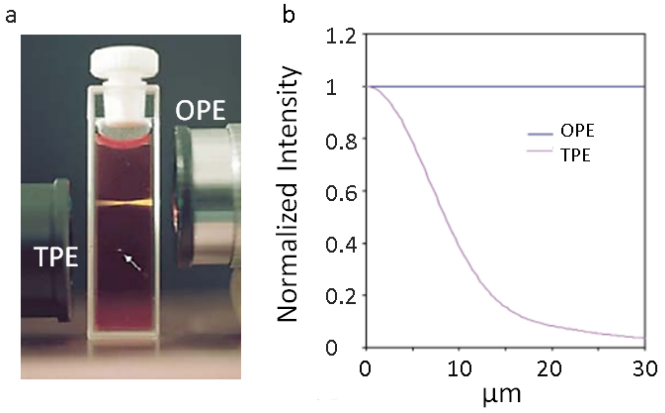

Figure 1.2
Comparison between the excitation profile and the out-of-focus fluorescence in one-photon and two-photon excitation. a) OPE and TPE excitation profiles in a fluorescent solution: while the OPE profile forms a line throughout the cuvet, the fluorescence of TPE occurs only within a small spot, indicated by the arrow. The picture is from [20]. b) Calculated fluorescence at different distances from the focal plane using an objective with numerical aperture = 0.1: within 10 µm the TP fluorescence decreases to 40%, while OP fluorescence hardly changes over several tens of microns. The figure is from [21].

izer, or grey filters. The beam is then scanned using a scanning mirror actuated by a piezo scanner. A scan lens converts the beam deflection into x-y movement. The scan lens is coupled to a second lens to adjust the beam size and direct it to the back aperture of the objective. When performing 3D imaging, a piezo stage is used to move the objective in the z direction. Alternatively the sample can be scanned by adjusting the focus. A dichroic mirror filters the reflected excitation light and directs the fluorescence to the detector.

For high resolution and high sensitivity, objectives with high numerical aperture (NA) are preferred. Higher NAs optimize the excitation efficiency by collecting light from a wider angle and confining the intensity to a smaller excitation volume. The optics used in a TP setup must be optimized for high power nIR light.

Though TP microscopes provide higher signal-to-noise ratio, deeper penetration into the sample, better 3D sectioning and less photodamage

compared to OP microscopes, a drawback common to both TP and OP confocal microscopes is the long acquisition time due to the sequential scanning.

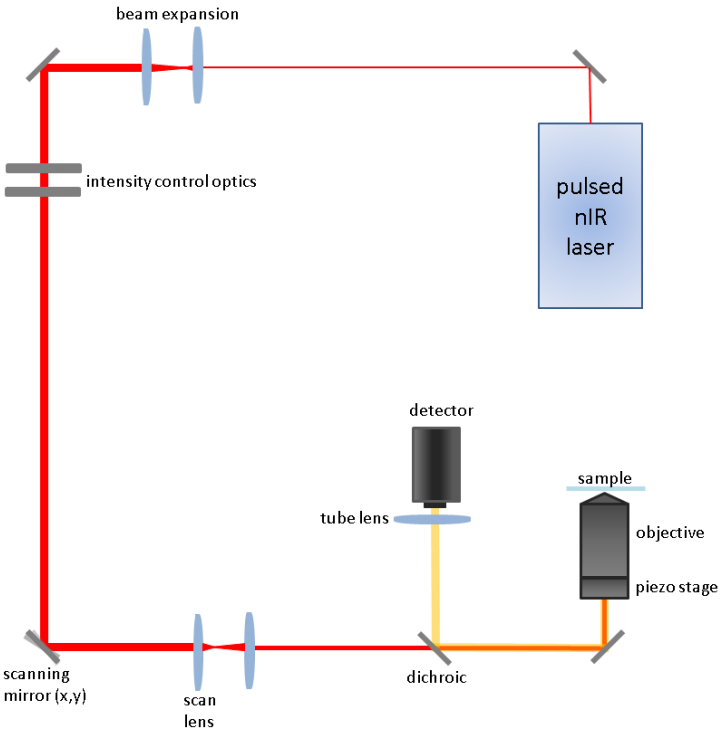

Figure 1.3
Basic scheme of a typical TP scanning microscope.

1.2.3 A two-photon multifocal scanning microscope

A way to reduce the acquisition time in a scanning microscope is to excite multiple foci in parallel. The first multifocal configuration was realized by Buist et al. [24] using a microlens array to create a 2D array of equidistant, diffraction-limited spots. However, the spots generated by microlenses in different parts of the array did not all have the same

intensity, resulting in a heterogeneous excitation pattern. A diffractive optical element (DOE) is a better solution, being able to generate a grid of spots of equal intensity [25].

For the experiments presented in this thesis we therefore used a two-photon multifocal scanning microscope exploiting a DOE. A scheme of the setup is shown in Fig. 1.4. This setup was presented previously by Van den Broek et al [26]. We made few modifications to the original scheme.

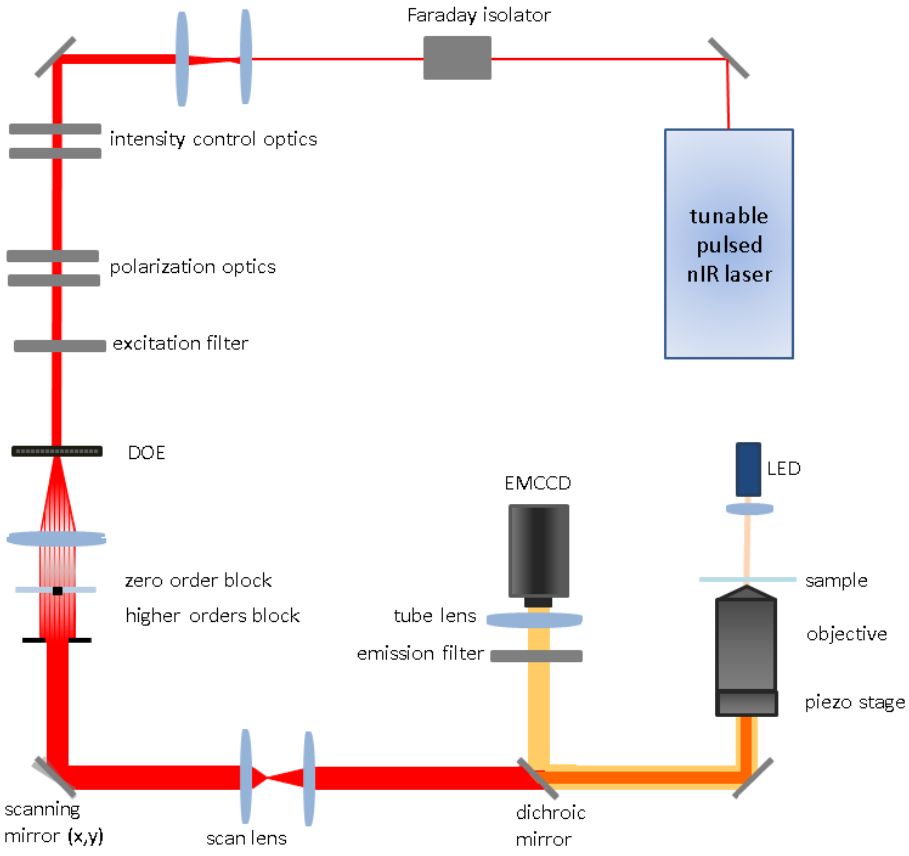

Figure 1.4
Scheme of a two-photon multifocal scanning microscope.

The excitation source is a Ti-Sa laser (Chameleon Ultra, Coherent, USA) with a pulse width of 140 fs at a rate of 80 MHz; the beam wavelength is automatically tunable in the range 690-1020 nm. A Faraday optical isolator (Broadband Faraday isolator, Newport, USA) prevents back-reflections from entering in the laser cavity. After expanding the beam with two lenses, the intensity is controlled by a $\lambda\backslash 2$ plate (WPH05M, Thorlabs, USA) and a beam splitter cube. Grey filters (NDA units, Thorlabs, USA) are used to further reduce the beam power. The diffractive optical element (custom-made by Holoeye Photonics, Germany) generates a 25x25 hexagonal array of focal spots. The beam is then collimated and sent through a glass coverslip, on to which a drop of solder alloy was deposited to block the zero order of the diffraction pattern. Orders of diffraction higher than the first one are filtered using a diaphragm. A $\lambda\backslash 4$ plate (WPQ05M, Thorlabs, USA) is used to convert the polarization of the light from linear to circular. A fast steering mirror (FSM-300, Newport) deflects the beam in two directions. The deflections are then converted to movements in the x and y plane by a scan lens. The beam is then expanded to fill the back aperture of the objective (Apo TIRF 60x, NA = 1.49, oil immersion, Nikon, Japan). A piezo-actuator (P-726, PIfoc, PI, Germany) moves the objective in the z direction to acquire 3D images. The sample is placed on an XY stage (PKTM50, Owis, Germany) driven by a stepper motor board (TMCM-610, Trinamic, Germany). A white light LED is used to obtain transmission images of the sample. The fluorescence light emitted by the sample is collected by the objective and deflected by a dichroic mirror (700dcxr, Chroma, USA) to an electron-multiplier-charged-coupled-device (EMCCD) camera (QuantEM 512SC, Photometrics, USA). An excitation filter (692LP, Semrock, USA) is placed before the dichroic, to block the residual visible light from the laser excitation. An emission filter (720SP, Semrock, USA) is placed before the tube lens, to block the residual excitation and scattering light. All the mirrors, filters and polarizers in the setup are optimized for high power nIR light.

The size of a pixel in the images acquired with this setup is 0.175 μm. The array of focal spots produced by the DOE (Fig. 1.5a) covers an area of approximately 350 x 350 pixels on the image, corresponding to about 60 μm x 60 μm. The distance between adjacent focal spots is approximately 17 pixels (about 3 μm). To obtain a homogeneous illumi-

nation of the sample, the scanning mirror is driven by an Archimedean spiral function, such that every focal spot develops into a 2D Gaussian profile. Scanning such a pattern was proven to provide the most homogeneous excitation pattern as compared to stochastic and raster scanning [26] (Fig. 1.6). The mirror scanner is synchronized with the camera exposure, to perform a complete spiral cycle within a single exposure (typically 50-100 ms). In the two directions, the Archimedean spiral function sent to the scanner is:

$$x = A\tau \sin(2\pi n\tau) \tag{1.1}$$

$$y = A\tau \cos(2\pi n\tau) \tag{1.2}$$

$$\tau = \sqrt{\frac{t}{T} \exp \frac{(t/T)^2}{2\sigma^2}} \tag{1.3}$$

where A is the amplitude of the scanning signal, n is the number of spiral branches, σ is the width of the Gaussian profile, and T is the exposure time of the camera. A homogenous excitation profile is obtained if the neighboring focal spots sufficiently overlap when scanned [26]. We obtained the most homogeneous excitation pattern using $A = 2$ μm, $\sigma =$ 1.4 μm and $n = 12$. The pattern obtained is shown in Fig. 1.5b.

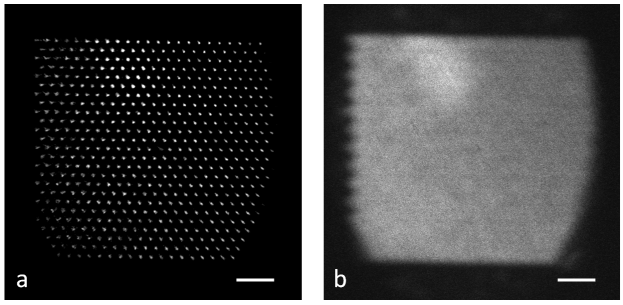

Figure 1.5
a) The 25x25 focal spots array generated by the DOE in our setup and b) the excitation profile obtained by scanning the array. The images are produced by reflecting the excitation beam with a mirror placed on the sample stage. The bottom right corner of the pattern is cut off along the beam path, due to the limited size of one of the mirrors. The bars in the images correspond to 10 μm.

The mirror scanner, the camera, the piezo actuator and the LED are connected to a data acquisition (DAQ) card (USB-6229, National Instrument, USA) that communicates between the computer and the devices. A LabVIEW program is used to synchronize the devices and acquire images.

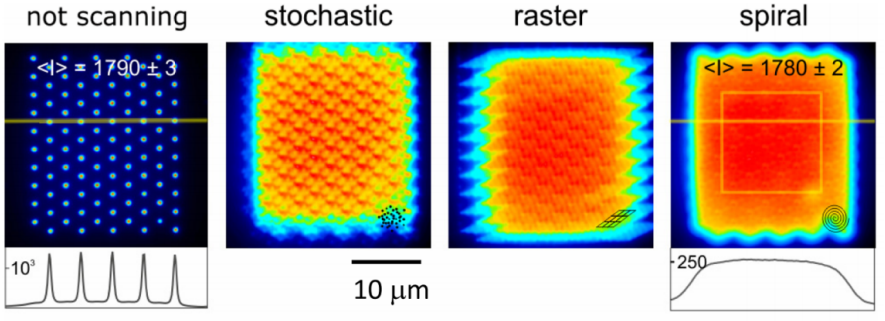

Figure 1.6
Comparison between stochastic, raster and spiral scanning. The image is from [26], where a 10x10 DOE was used to generate a grid of focal spots. Spiral scanning provides the most homogeneous distribution of the intensity.

1.3 Metal nanoparticles

In the first section of this chapter we presented the possible labels for SM imaging experiments: fluorescent proteins, organic dyes and nanoparticles. For our experiments we chose a particular kind of nanoparticles: gold nanorods. Here we discuss the optical properties that make metal nanoparticles in general, and gold nanorods in particular, so advantageous for SM imaging.

1.3.1 Surface plasmons, absorption and scattering

When a noble metal particle is irradiated by an external electric field, a collective oscillation of the free conduction electrons on the surface is generated. This oscillation is called surface plasmon (SP). During

the oscillation, the electron cloud moves away from the nuclei in the lattice, and a restoring force is generated by the Coulomb interactions between the nuclei and the displaced electrons (Fig 1.7a). Plasmons are therefore dipole oscillations. Multipole oscillations can also occur, such as quadrupole oscillations: one half of the electrons moves parallel to the excitation field and the other half moves antiparallel [27].

The plasmon excitation decays through a non-radiative or radiative pathway. Non-radiative pathways include energy transfer to the lattice or to the environment. Radiative decay occurs by recombination of the electrons with the holes in the lattice, with consequent emission of photons. The probability of radiative decay is low, due to the high efficiency of the non-radiative processes.

As opposed to fluorescent proteins and dyes, in metal nanoparticles all the surface electrons participate in the plasmonic oscillation. This makes the extinction (absorption + scattering) cross-section very large. The absorption and scattering cross sections of metal nanoparticles can be up to respectively 5-6 and 4-5 orders of magnitude larger than the cross-sections of organic dyes [28, 29]. In addition, noble metals do not react with the environment, resulting in a more stable signal compared to the signal from organic dyes and fluorescent proteins. Therefore, bleaching and blinking are generally not an issue when using these nanoparticles as labels.

A theoretical description of surface plasmons was presented by Mie [30, 31]. Solving the Maxwell equations to calculate the scattering produced by an irradiated sphere, he obtained a field that can be approximated by a dipole. This dipole is the plasmon oscillation. The dipole approximation is valid when the particle is much smaller than the wavelength of the incident light, like in case of nanoparticles.

The polarizability of a spherical metal particle is:

$$\alpha = 4\pi r^3 \epsilon_0 \frac{\epsilon_\lambda - \epsilon_0}{\epsilon_\lambda + 2\epsilon_0} \tag{1.4}$$

where r is the radius of the particle, ϵ_0 the dielectric constant of the medium and ϵ_λ the dielectric constant of the particle that depends on the wavelength of the incoming light λ. For $\epsilon_\lambda = -2\epsilon_0$ the polarizability is maximal and a resonant dipole oscillation is established in the particle. This condition is referred to as surface plasmon resonance (SPR) and is satisfied for a particular wavelength value. For gold spheres, the

SPR wavelength is around 520 nm (Fig. 1.7b). In Mie's approximation the SPR is independent from the particle size. Experimentally, a weak dependence of the SPR on the size of a gold sphere was found [32, 33] (Fig. 1.8).

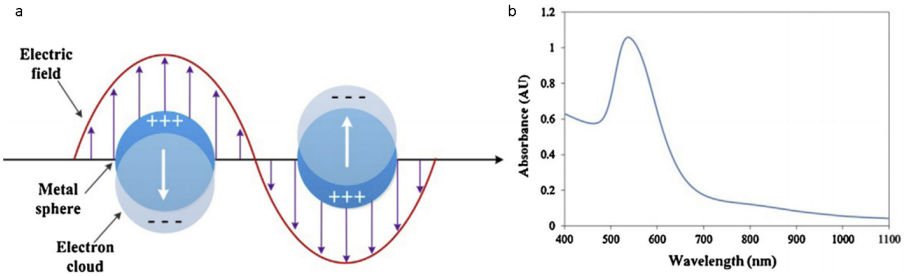

Figure 1.7
Surface plasmon resonance in a metal nanosphere. a) The plasmons enhance the absorption cross-section, resulting in a peak in the absorption spectrum (shown in b) at the plasmon resonance wavelength. The figure is from [32].

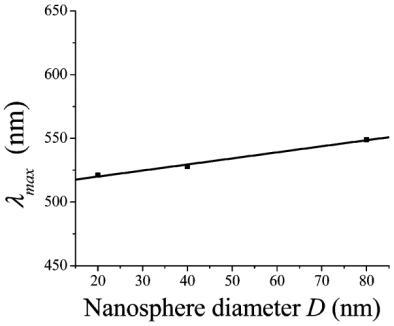

Figure 1.8
Dependence of the plasmon resonance peak on the sphere size. The figure is from [33].

The absorption and the scattering cross sections of the particle are functions of the polarizability [34]:

$$\sigma_{ext} = \sigma_{scat} + \sigma_{abs} \tag{1.5}$$

$$\sigma_{scat} = \left(\frac{2\pi}{\lambda}\right)^4 \frac{|\alpha^2|}{6\pi} \tag{1.6}$$

$$\sigma_{abs} = \frac{2\pi}{\lambda} Im(\alpha) \tag{1.7}$$

which has a maximum in the resonance condition (see Eq. 1.4). Consequently, the absorption and scattering spectra feature a peak at the SPR energy (Fig. 1.7b).

Combining Eq. 1.4 with Eq. 1.6, 1.7 shows the dependence of absorption and scattering cross-section from the size of the particle. As the particle size increases, the contribution of scattering in the exctinction cross-section becomes dominant. Smaller particles are thus more suitable for applications involving absorption, while bigger particles are used for scattering applications [34].

The dipole approximation presented here is valid for particles smaller than about 50 nm. For larger particles the external electric field cannot be considered constant and the contribution of higher modes of oscillation increases [35].

1.3.2 Gold nanorods

Among noble metal nanoparticles, gold nanoparticles are easy to synthetize and conjugate to biomolecules and present low toxicity due to the lower reactivity and lower release of free ions compared to silver and copper nanoparticles [32, 33].

Among gold nanoparticles, gold nanorods (GNRs) are commonly used. The synthesis of GNRs is well established and they present some advantages over nanospheres. Nanorods have two different plasmon oscillation modes: a longitudinal one and a transversal one. The transversal mode, corresponding to the oscillations of electrons in the direction of the two shorter axes, has the same energy as the plasmon of a nanosphere. The longitudinal plasmon, corresponding to the electronic oscillation in the direction of the longer axis of the rod, appears at higher wavelengths (Fig. 1.9).

The optical properties of gold nanorods were derived by Gans, using a version of Mie's theory that approximates rods to prolate ellipsoids.

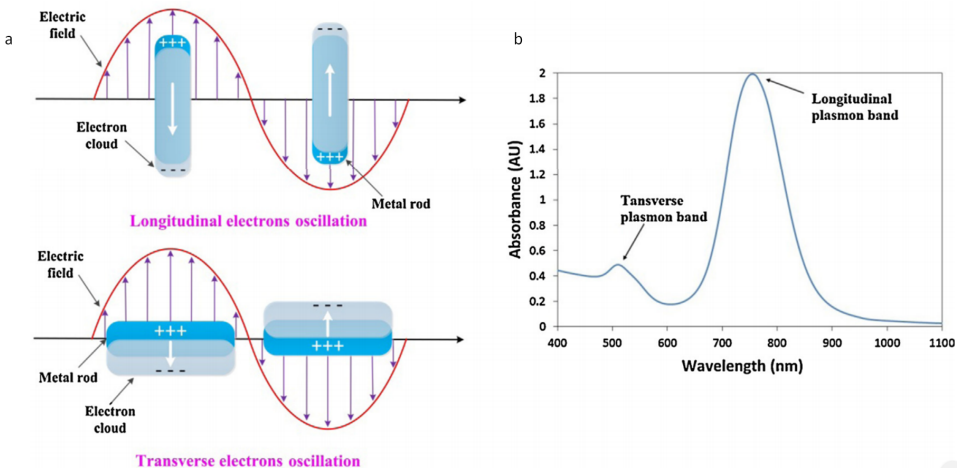

Figure 1.9
a) Surface plasmon resonance in a nanorod: the longitudinal and transversal electron oscillations in the particle generate two peaks in the absorption spectrum (shown in b)). The figure is from [33].

In Gans's calculation, the polarizability of an ellipsoid under irradiation parallel to one of its axes i is [36, 37]:

$$\alpha_i = 4\pi V \frac{\epsilon_\lambda - \epsilon_0}{\epsilon_0 + L_i(\epsilon_\lambda - \epsilon_0)} \tag{1.8}$$

where V is the volume of the particle and L_i are the depolarization factors for each axis (for the spherical case, $L_i = 1/3$). Defining a as the longer axis and $b{=}c$ the shorter axes, L_i are defined as:

$$L_a = \frac{2}{R^2-1}\left(\frac{R}{R^2-1} ln \frac{R+\sqrt{R^2-1}}{R-\sqrt{R^2-1}} - 1\right) \tag{1.9}$$

$$L_{b,c} = \frac{1-L_a}{2} \tag{1.10}$$

L_a is the depolarization along the long axis, and $L_{b,c}$ are the depolarizations along the two short axes; R is the aspect ratio of the particle, defined as a/b. Combining Eq. 1.8 with Eq. 1.9 and 1.10 shows that the polarization in a nanorod depends not only on the dielectric constants of the particle and of the medium, but also on the aspect ratio of the

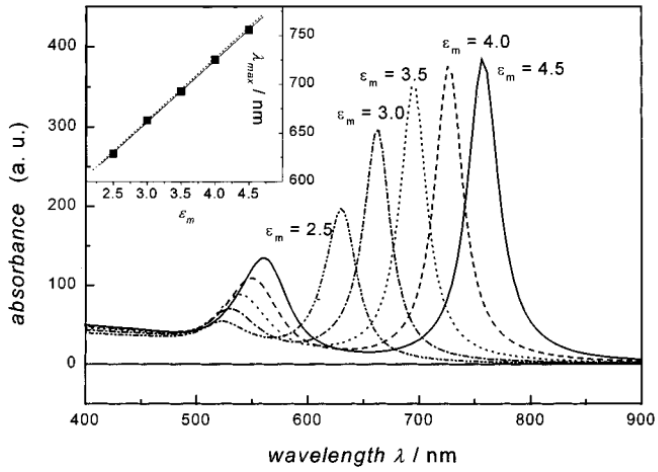

Figure 1.10
Dependence of the absorption peaks of nanorods from the dielectric constant of the environment. A linear dependence (inset) is obtained for the longitudinal peak. The figure is from [39].

particle.

The absorption and scattering cross-sections of rods are [38]:

$$\sigma_{abs} = \frac{2\pi}{3\lambda} V {\epsilon_0}^{3/2} \sum i \frac{\frac{\mathrm{Im}(\epsilon)}{L_i^2}}{\mathrm{Re}(\epsilon) + \epsilon_0 \frac{1-L_i}{L_i}^2 + \mathrm{Re}(\epsilon)^2} \tag{1.11}$$

$$\sigma_{scat} = \frac{8\pi^3}{9\lambda^4} V^2 {\epsilon_0}^2 \sum i \frac{\frac{\mathrm{Re}(\epsilon)-\epsilon_0{}^2+\mathrm{Im}(\epsilon)^2}{L_i^2}}{\mathrm{Re}(\epsilon) + \epsilon_0 \frac{1-L_i}{L_i}^2 + \mathrm{Im}(\epsilon)^2} \tag{1.12}$$

Due to the resonance condition, the absorption and scattering cross-sections depend on the dielectric constant of the particle and of the medium (Fig. 1.10).

Having a larger polarizability, the longitudinal plasmon presents a stronger dependence on the size of the GNR, while the transversal plasmon is only weakly dependent on the particle shape, as in the case of nanospheres. In particular, the resonant wavelength of the longitudinal plasmon red-shifts for increasing aspect ratios [39] (Fig. 1.11a). It is

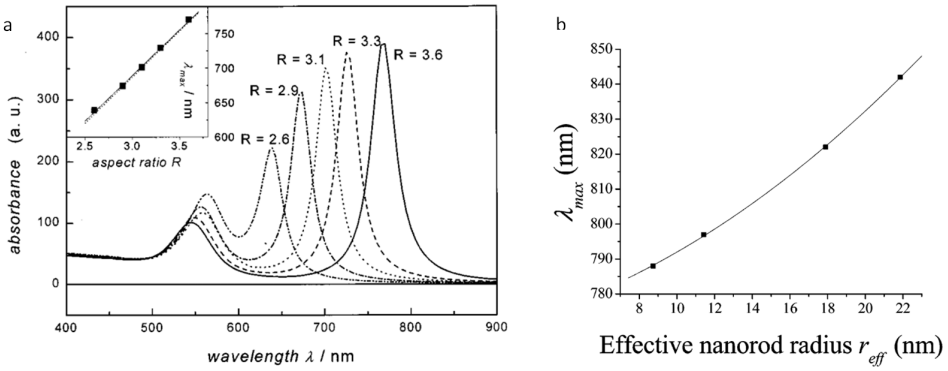

Figure 1.11
Dependence of the longitudinal peak on the shape and size of the GNR. a) Red shift of the longitudinal plasmon wavelength for increasing aspect ratios. The dependence is linear (inset). The figure is from [39]. b) Absorption peak for nanorods with different effective radius, at constant aspect ratio $R = 3.9$. The figure is from [33].

thus possible to synthesize nanorods with a range of longitudinal plasmon wavelengths by tuning their aspect ratio, up to the nIR region of the light spectrum. In this region, especially within the 650-1350 nm window, the damage caused by light in tissues in minimized, making gold nanoparticles very useful for biological applications [31].

The dependence of the longitudinal mode on the volume of the particle is stronger than in nanospheres: this dependence can be expressed in terms of GNR effective radius, defined as the radius of a sphere with equivalent volume (Fig. 1.11b). The longitudinal plasmon exhibits also a stronger dependence on the dielectric constant of the particle and the environment, making gold nanorods useful for sensing purposes.

A final advantage of nanorods over nanospheres is the dependence of absorption and emission on the polarization of the light. It is then possible to detect different orientation of the nanorods and study rotational dynamics. While the spectrum of a nanosphere is independent from the polarization of the excitation light, the scattering spectrum of GNRs shows a $\cos^2$ dependence (Fig. 1.12).

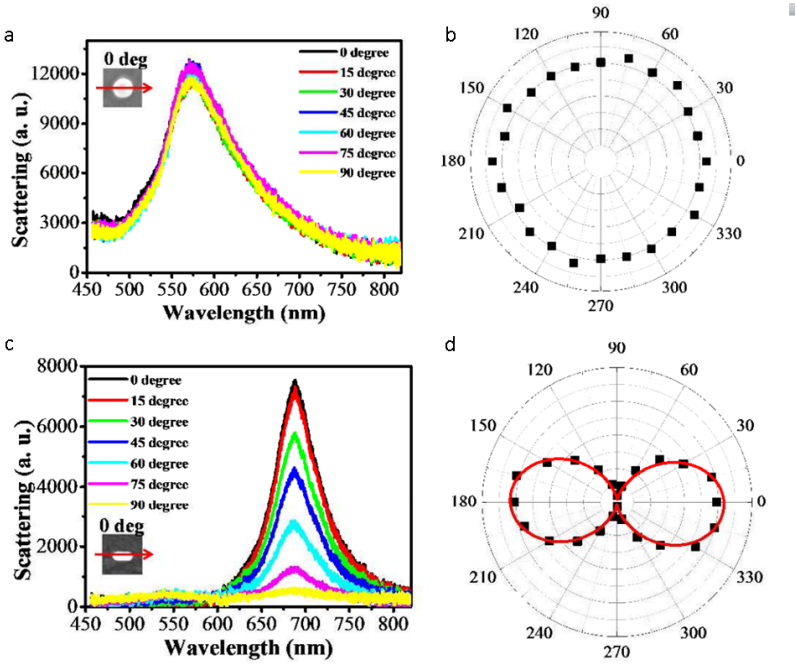

Figure 1.12
Scattering spectra of a) a nanosphere and b) a nanorod excited under light with varying polarization. The scattering intensity exhibits no dependence on the polarization in case of nanospheres, and a cos^2 dependence in case of nanorods. The image is from [40].

Similarly to nanospheres, scattering dominates for larger nanorods and absorption for smaller ones [41] (Fig. 1.13). Therefore larger GNRs may be more suitable for imaging experiments, while small ones are preferred for applications using absorption and heating [42]. In our experiments, we chose gold nanorods with sizes ranging from about 40 nm x 10 nm to 60 nm x 20 nm. This size may be rather large for applications in which a single protein is labeled and tracked in a cell. Moreover, in such a crowded environment a large size leads to an increased possibility of getting stuck as compared to smaller particles. However, nanorods of this size provide an exceptional brightness and consequently very high localization accuracy inside the cell.

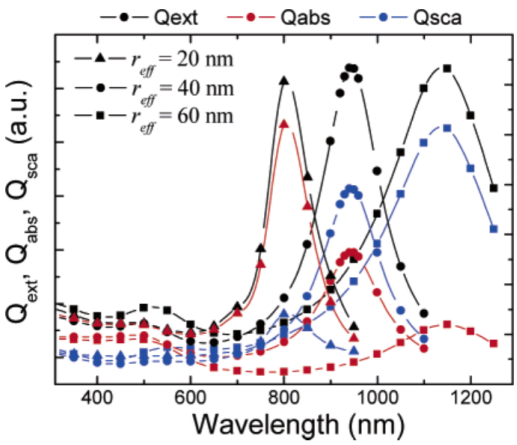

Figure 1.13
The relative contribution of absorption and scattering to the exctinction cross-section depends on the GNR size. The figure is from [41].

1.4 Photoluminescence of gold nanorods

1.4.1 One-photon photoluminescence

In our experiments we image gold nanorods taking advantage of their two-photon photoluminescence. In this section we discuss the origin of the photoluminescence of gold nanoparticles, both in one-photon and in two-photon.

Bulk gold exhibits a weak photoluminescence, that can be explained as the result of a three-steps process [43]:

1. Upon light irradiation, the electrons in the d band are excited and migrate to the sp or d conduction band, generating electron-hole couples.

2. The electrons relax, losing energy via scattering with other electrons or phonons

3. The excited electrons can recombine with holes in the d band, causing emission of photons.

The energy levels in metals are more closely spaced than in molecules, and excited electrons can relax till the lowest energy above the Fermi level. The relaxation processes are faster than electron-pair recombinations, hence the low quantum yield of gold (about 10^{-10}). However, an enhancement by several orders of magnitudes is obtained by increasing the surface roughness of the metal [44]. This enhancement is due to the "lighting-rod effect": a rough surface has protrusions where the electron motions gets confined, establishing local surface plasmons. This also occurs in nanoparticles [45]: in gold nanorods an increase in quantum yield of a million times was observed, compared to bulk gold. Surface plasmons enhance both the recombination rate between electrons and holes and the photon emission, resulting in increased absorption and luminescence efficiency [46]. Therefore, the photoluminescence process in metal nanoparticles, though excited at any energy, is strongly enhanced by SPR [47]. As a consequence, the photoluminescence spectrum overlaps with the scattering and absorption spectrum [48], as shown in Fig. 1.14.

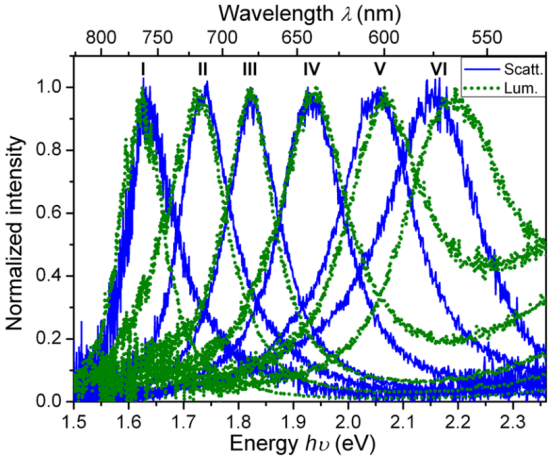

Figure 1.14
Correlation between the scattering (blue continuous line) and one photon luminescence spectrum (green dotted line) of GNRs with different aspect ratios. The figure is from [48].

The same dependence on the aspect ratio of the rods and on the dielectric constant of the environment has been reported [45, 46].

In GNRs, the luminescence quantum yield is weakly dependent on the volume. In large rods a slight decrease of the quantum efficiency was observed and was explained by partial reabsorption of the radiation by the particles [48].

1.4.2 Two-photon photoluminescence

In addition to one-photon luminescence, gold nanorods exhibit strong two-photon photoluminescence (TPPL). This phenomenon can be explained as a process involving two sequential one-photon steps [49–51] (Fig. 1.15):

1. Upon light excitation, the first photon excites an intraband transition within the sp band, from below to above the Fermi level, creating a hole.

2. The second photon excites an electron in the d band to recombine with the sp hole left from the first excitation, creating a second hole in the d band. The excited electron in the sp band can now recombine with the hole in the d band, emitting a photon.

Therefore, similar to one-photon luminescence, TPPL is also enhanced by SPR. The TPPL spectrum overlaps with the OP and scattering spectrum (Fig 1.16, [52]) and depends on the aspect ratio of the nanorod and on the dielectric constant of the medium.

TPPL exhibits a quadratic dependence on the excitation intensity, resulting in a narrower TP spectrum than the scattering spectrum (Fig. 1.17a). In sensing applications, it is important to precisely localize the peak in the spectrum of a GNR, to be able to detect small variations in its position due for example to the interaction with a molecule. Using TP spectra can thus be advantageous over OP and scattering spectra.

As a consequence of quadratic dependence on the excitation, TPPL is proportional to the $\cos^4$ of the polarization of the excitation light (Fig. 1.17b).

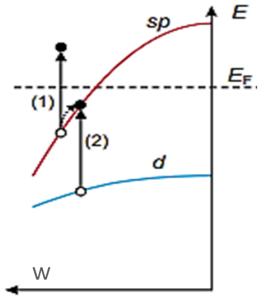

Figure 1.15
TPPL excitation process in GNRs. Excitation of one electron from the sp band to above the Fermi level and excitation of another electron from the d band to the sp band. The x and y axes indicate the wave number and the energy of the electronic levels. The figure is from [51].

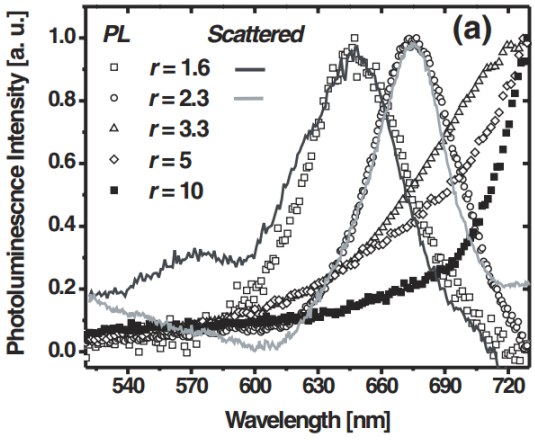

Figure 1.16
Correlation between the scattering (lines) and the TPPL spectra (dots) for GNRs with different aspect ratios. The figure is from [52].

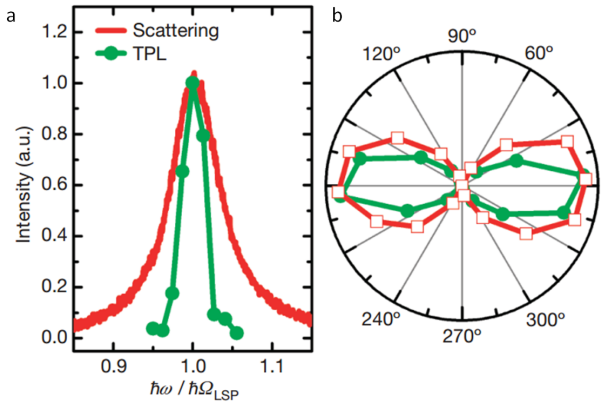

Figure 1.17
a) Comparison between the scattering (red line) and the TPPL spectrum (green dots and line) of a gold nanorod and b) dependence of their intensities from the polarization of the incident light. The figure is from [53].

1.5 Outline of the thesis

In this thesis we applied the two-photon photoluminescence of gold nanorods in single-particle tracking and spectroscopy experiments, using a multifocal scanning microscope.

In **Chapter 2** we characterized the accuracy of our microscope in localizing GNRs and detecting their diffusion. The precision of single-particle tracking results depends on the features of the setup and the stochasticity intrinsic to diffusion. Using simulations and experiments *in vitro*, we adjusted the parameters used in mean squared displacement analysis to obtain the most accurate measure of diffusion. We applied the analysis to the detection of temporal changes in the simulated diffusion of a GNR, mimicking a transient binding process as it can occur between a protein and a cellular structure. The results show how the detection of the event depends on the mobility of the ligands and of the duration of the binding event.

In **Chapter 3** we explored the use of GNRs for single-particle tracking in living cells. We first tested different delivery techniques in three different cell types. For each delivery technique we evaluated the delivery efficiency and the short-term effect on cell viability. We then analyzed the mobility of the GNRs delivered with each method. We observed immobile GNRs, freely diffusing GNRs and GNRs diffusing within confined areas inside the cells. The quantification of mobility parameters yielded similar results for GNRs delivered with all successful techniques, though delivery efficiency and cell viability varied. Interestingly, GNRs showed a similar mobility in the cytoplasm and in the nucleus of cells.

The final goal of single-particle tracking of GNRs is to follow biomolecules inside cells. To this aim, they need to be specifically functionalized. As described in **Chapter 4**, we functionalized GNRs with nuclear localization signal peptides which induce nuclear targeting. We analyzed the localization of the GNRs inside the cell, and quantified the efficiency of nuclear targeting of functionalized GNRs as compared to GNRs without the peptides. We obtained a low nuclear delivery efficiency that we attributed to the large size of the GNRs used for the experiment. We then analyzed the mobility of functionalized GNRs, that yielded similar results to the ones obtained previously with non-functionalized GNRs.

In **Chapter 5** we explored the use of GNRs for spectroscopy applications. Our setup allows for fast tuning of the laser wavelength, and can be used to acquire two-photon excitation spectra of many GNRs in parallel. The spectra we obtained showed unexpected features, not compatible with single GNRs. We tested several hypotheses to explain the origin of such spectra, and pinpointed the elements in the setup which my underlie the modulation in the signal. We could not perform sensing experiments yet, but the experiments we presented were a necessary step towards the acquisition of TP spectra of single gold nanorods with our setup.

Bibliography

[1] WE Moerner and L Kador. "Optical detection and spectroscopy of single molecules in a solid." In: *Physical review letters* 62.21 (May 1989), pp. 2535–2538. ISSN: 1079-7114.

[2] M Orrit and J Bernard. "Single pentacene molecules detected by fluorescence excitation in a p-terphenyl crystal." In: *Physical review letters* 65.21 (Nov. 1990), pp. 2716–2719. ISSN: 1079-7114.

[3] T Funatsu et al. "Imaging of single fluorescent molecules and individual ATP turnovers by single myosin molecules in aqueous solution." In: *Nature* 374.6522 (Apr. 1995), pp. 555–9. ISSN: 0028-0836.

[4] S Weiss. "Measuring conformational dynamics of biomolecules by single molecule fluorescence spectroscopy." eng. In: *Nature structural biology* 7.9 (Sept. 2000), pp. 724–9. ISSN: 1072-8368.

[5] G J Schutz et al. "Properties of lipid microdomains in a muscle cell membrane visualized by single molecule microscopy." In: *The EMBO journal* 19.5 (Mar. 2000), pp. 892–901. ISSN: 0261-4189.

[6] Akihiko Ishijima and Toshio Yanagida. "Single molecule nanobioscience". In: *Trends in Biochemical Sciences* 26.7 (July 2001), pp. 438–444. ISSN: 09680004.

[7] Y Sako, S Minoghchi, and T Yanagida. "Single-molecule imaging of EGFR signalling on the surface of living cells." In: *Nature cell biology* 2.3 (Mar. 2000), pp. 168–72. ISSN: 1465-7392.

[8] Hideji Murakoshi et al. "Single-molecule imaging analysis of Ras activation in living cells." In: *Proceedings of the National Academy of Sciences of the United States of America* 101.19 (May 2004), pp. 7317–22. ISSN: 0027-8424.

[9] Adam D Douglass and Ronald D Vale. "Single-molecule imaging of fluorescent proteins." In: *Methods in cell biology* 85 (Jan. 2008), pp. 113–25. ISSN: 0091-679X.

[10] G S Harms et al. "Autofluorescent proteins in single-molecule research: applications to live cell imaging microscopy." In: *Biophysical journal* 80.5 (May 2001), pp. 2396–408. ISSN: 0006-3495.

[11] M Sameiro T Gonçalves. "Fluorescent labeling of biomolecules with organic probes." In: *Chemical reviews* 109.1 (Jan. 2009), pp. 190–212. ISSN: 1520-6890.

[12] Ute Resch-Genger et al. "Quantum dots versus organic dyes as fluorescent labels." In: *Nature methods* 5.9 (Sept. 2008), pp. 763–75. ISSN: 1548-7091.

[13] Irwin Chen and Alice Y Ting. "Site-specific labeling of proteins with small molecules in live cells." In: *Current opinion in biotechnology* 16.1 (Feb. 2005), pp. 35–40. ISSN: 0958-1669.

[14] I Sase et al. "Real time imaging of single fluorophores on moving actin with an epifluorescence microscope." In: *Biophysical journal* 69.2 (Aug. 1995), pp. 323–8. ISSN: 0006-3495.

[15] V Hlady, D.R Reinecke, and J.D Andrade. "Fluorescence of adsorbed protein layers". In: *Journal of Colloid and Interface Science* 111.2 (June 1986), pp. 555–569. ISSN: 00219797.

[16] Fritjof Helmchen and Winfried Denk. "Deep tissue two-photon microscopy". In: 2.12 (2005).

[17] W Denk, J. Strickler, and W. Webb. "Two-photon laser scanning fluorescence microscopy". In: *Science* 248.4951 (Apr. 1990), pp. 73–76. ISSN: 0036-8075.

[18] V E Centonze and J G White. "Multiphoton excitation provides optical sections from deeper within scattering specimens than confocal imaging." In: *Biophysical journal* 75.4 (Oct. 1998), pp. 2015–24. ISSN: 0006-3495.

[19] Patrick Theer, Mazahir T. Hasan, and Winfried Denk. "Two-photon imaging to a depth of 1000 um in living brains by use of a Ti:Al_2O_3 regenerative amplifier". EN. In: *Optics Letters* 28.12 (June 2003), p. 1022. ISSN: 0146-9592.

[20] Alberto Diaspro, Giuseppe Chirico, and Maddalena Collini. "Two-photon fluorescence excitation and related techniques in biological microscopy." English. In: *Quarterly reviews of biophysics* 38.2 (May 2005), pp. 97–166. ISSN: 0033-5835.

[21] Peter T C So et al. “Two-Photon Excitation Fluorescence Microscopy”. In: (2000), pp. 399–429.

[22] G H Patterson and D W Piston. “Photobleaching in two-photon excitation microscopy.” In: *Biophysical journal* 78.4 (Apr. 2000), pp. 2159–62. ISSN: 0006-3495.

[23] Joon Myong Song et al. “Determination of Two Photon Absorption Cross Section of Fluorescein Using a Mode Locked Titanium Sapphire Laser.” In: *Analytical Sciences* 15.6 (1999), pp. 601–603. ISSN: 0910-6340.

[24] Buist et al. “Real time two-photon absorption microscopy using multi point excitation”. In: *Journal of Microscopy* 192.2 (Nov. 1998), pp. 217–226. ISSN: 0022-2720.

[25] L. Sacconi et al. “Multiphoton multifocal microscopy exploiting a diffractive optical element”. EN. In: *Optics Letters* 28.20 (Oct. 2003), p. 1918. ISSN: 0146-9592.

[26] Bram van den Broek et al. “Parallel nanometric 3D tracking of intracellular gold nanorods using multifocal two-photon microscopy.” In: *Nano letters* 13.3 (Mar. 2013), pp. 980–6. ISSN: 1530-6992.

[27] K. Lance Kelly et al. “The Optical Properties of Metal Nanoparticles: The Influence of Size, Shape, and Dielectric Environment”. In: *The Journal of Physical Chemistry B* 107.3 (Jan. 2003), pp. 668–677. ISSN: 1520-6106.

[28] Prashant K Jain et al. “Noble metals on the nanoscale: optical and photothermal properties and some applications in imaging, sensing, biology, and medicine.” In: *Accounts of chemical research* 41.12 (Dec. 2008), pp. 1578–86. ISSN: 1520-4898.

[29] Huanjun Chen et al. “Gold nanorods and their plasmonic properties.” en. In: *Chemical Society reviews* 42.7 (Apr. 2013), pp. 2679–724. ISSN: 1460-4744.

[30] Gustav Mie. “Beitrage zur Optik truber Medien, speziell kolloidaler Metallosungen”. In: *Annalen der Physik* 330.3 (1908), pp. 377–445. ISSN: 00033804.

[31] R Weissleder. “A clearer vision for in vivo imaging.” In: *Nature biotechnology* 19.4 (Apr. 2001), pp. 316–7. ISSN: 1087-0156.

[32] Saumyakanti Khatua and Michel Orrit. "Probing, Sensing, and Fluorescence Enhancement with Single Gold Nanorods." In: *The journal of physical chemistry letters* 5.17 (Sept. 2014), pp. 3000–6. ISSN: 1948-7185.

[33] Prashant K Jain et al. "Calculated Absorption and Scattering Properties of Gold Nanoparticles of Different Size, Shape, and Composition: Applications in Biological Imaging and Biomedicine". In: *The Journal of Physical Chemistry* (2006).

[34] Meindert Alexander van Dijk and Faculteit der Wiskunde en Natuurwetenschappen. *Nonlinear optical studies of single gold nanoparticles*. en.

[35] P Zijlstra and M Orrit. "Single metal nanoparticles: optical detection, spectroscopy and applications". en. In: *Reports on Progress in Physics* 74.10 (Oct. 2011), p. 106401. ISSN: 0034-4885.

[36] R. Gans. "Uber die Form ultramikroskopischer Goldteilchen". In: *Annalen der Physik* 342.5 (1912), pp. 881–900. ISSN: 00033804.

[37] Craig F. Bohren and Donald R. Huffman. *Absorption and Scattering of Light by Small Particles*. Weinheim, Germany: Wiley-VCH Verlag GmbH, Apr. 1983. ISBN: 9783527618156.

[38] Xiaohua Huang, Svetlana Neretina, and Mostafa A. El-Sayed. "Gold Nanorods: From Synthesis and Properties to Biological and Biomedical Applications". In: *Advanced Materials* 21.48 (Dec. 2009), pp. 4880–4910. ISSN: 09359648.

[39] S. Link, M. B. Mohamed, and M. A. El-Sayed. "Simulation of the Optical Absorption Spectra of Gold Nanorods as a Function of Their Aspect Ratio and the Effect of the Medium Dielectric Constant". In: *The Journal of Physical Chemistry B* 103.16 (Apr. 1999), pp. 3073–3077. ISSN: 1520-6106.

[40] Nengyue Gao et al. "Shape-Dependent Two-Photon Photoluminescence of Single Gold Nanoparticles". In: *The Journal of Physical Chemistry C* (June 2014), p. 140611092005007. ISSN: 1932-7447.

[41] Kyeong-Seok Lee and Mostafa A El-Sayed. "Dependence of the enhanced optical scattering efficiency relative to that of absorption for gold metal nanorods on aspect ratio, size, end-cap shape, and medium refractive index." In: *The journal of physical chemistry. B* 109.43 (Nov. 2005), pp. 20331–8. ISSN: 1520-6106.

[42] Moustafa R K Ali, Brian Snyder, and Mostafa a El-Sayed. "Synthesis and optical properties of small Au nanorods using a seedless growth technique." In: *Langmuir : the ACS journal of surfaces and colloids* 28.25 (June 2012), pp. 9807–15. ISSN: 1520-5827.

[43] A. Mooradian. "Photoluminescence of Metals". In: *Physical Review Letters* 22.5 (Feb. 1969), pp. 185–187. ISSN: 0031-9007.

[44] G. T. Boyd, Z. H. Yu, and Y. R. Shen. "Photoinduced luminescence from the noble metals and its enhancement on roughened surfaces". In: *Physical Review B* 33.12 (June 1986), pp. 7923–7936. ISSN: 0163-1829.

[45] Mona B. Mohamed et al. "The 'lightning' gold nanorods: fluorescence enhancement of over a million compared to the gold metal". In: *Chemical Physics Letters* 317.6 (Feb. 2000), pp. 517–523. ISSN: 00092614.

[46] Susie Eustis and Mostafa El-Sayed. "Aspect ratio dependence of the enhanced fluorescence intensity of gold nanorods: experimental and simulation study." In: *The journal of physical chemistry. B* 109.34 (Sept. 2005), pp. 16350–6. ISSN: 1520-6106.

[47] Da-Shin Wang, Fu-Yin Hsu, and Chii-Wann Lin. "Surface plasmon effects on two photon luminescence of gold nanorods". In: *Optics Express* 17.14 (June 2009), p. 11350. ISSN: 1094-4087.

[48] Mustafa Yorulmaz et al. "Luminescence quantum yield of single gold nanorods." In: *Nano letters* 12.8 (Aug. 2012), pp. 4385–91. ISSN: 1530-6992.

[49] Haifeng Wang et al. "In vitro and in vivo two-photon luminescence imaging of single gold nanorods." In: *Proceedings of the National Academy of Sciences of the United States of America* 102.44 (Nov. 2005), pp. 15752–6. ISSN: 0027-8424.

[50] Kohei Imura, Tetsuhiko Nagahara, and Hiromi Okamoto. "Near-field two-photon induced photoluminescence from single gold nanorods and imaging of plasmon modes." In: *The journal of physical chemistry. B* 109.27 (July 2005), pp. 13214–20. ISSN: 1520-6106.

[51] P. Biagioni et al. "Dependence of the two-photon photoluminescence yield of gold nanostructures on the laser pulse duration". In: *Physical Review B* 80.4 (July 2009), p. 045411. ISSN: 1098-0121.

[52] A. Bouhelier et al. “Surface Plasmon Characteristics of Tunable Photoluminescence in Single Gold Nanorods”. In: *Physical Review Letters* 95.26 (Dec. 2005), pp. 4–7. ISSN: 0031-9007.

[53] Peter Zijlstra, James W M Chon, and Min Gu. “Five-dimensional optical recording mediated by surface plasmons in gold nanorods.” In: *Nature* 459.7245 (May 2009), pp. 410–3. ISSN: 1476-4687.